4
Effects of Gamma Irradiation on Structural and Surface Chemical Properties of $BaSrTiO_3$ Thin Film

4.1 INTRODUCTION

Recently growth of complex oxides thin film has attarcated lot of attention to understand basic science for various applications including tunable varactors [Subramanyam *et al*, 2013]. The device performance and the physical properties such as polarization, dielectric behavior and their dc leakage current are closely linked to the microstructure and the interfaces between the succeding layers. It is therefore desirable to fabricate these thin films and investigate their structural and microstructural features. In addition to this, the deposition parameters like substrate temperature and sputtring gas pressure does play an important role in stabilizing microstructural feature and hence physical properties. Therefore, optimizations of film growth parameters are necessary in order to achieve good quality thin films with desired functional properties. Barium titanate ($BaTiO_3$) is a ferroelectric perovskite material and has been well investigated in bulk ceramics where the measured permittivity is in order of thousand. A-site atom (Ba-atom) can be substituted with Sr to improve the tunable characteristics of the device with shifting of curie temperature near to room temperature. $BaSrTiO_3$ (BST) was found an attractive candidate for voltage tunable devices, phase shifters, varactors, etc. Their properties storngly depend on stoichiometry, microstructure, film thickness and homogeneity of the film. Moreover, film dielectric properties are governed by growth method composition, stoichiometry and crystallinity. $(Ba_{0.5},Sr_{0.5})TiO_3$ was chosen as a thin film material in this study as it is widely used material in voltage unable device along with its high dielectric constant [Miyasaka and Matsubara, 1990].

In this chapter we have optimised growth parameters for deposition of $Ba_{0.5}Sr_{0.5}TiO_3$ on silicon (Si) substrate by RF magnetron sputtering technique in order to study gamma radiation induced structural changes in the film. The substrate temperature and sputtered gas flow rate play a crucial role in deciding the phase formation and the microstructure of the thin film. The BST thin films have also been investigated for gamma radiation effects on surface properties mainly for chemical states and surface morphologies. In addition, leakage current for different gamma doses were also measured to support formation of oxygen vacancy after irradiation. The detailed thin film growth procedure and their structural and microstructural characterization are discussed in next sections.

4.2 OPTIMISATION OF DEPOSITION PARAMETERS FOR BST THIN FILMS

RF magnetron sputtering technique has been used to deposit $Ba_{0.5}Sr_{0.5}TiO_3$ (BST) thin film. The deposition chamber is evacuated and Ar gas is introduced in the chamber at low pressure. After applying AC voltage, glow-discharge plasma occured between the target (cathode) and anode. By using prinicple of momentum exchange, target atoms are sputtered by accelerated positive Ar ions in the chamber. The film is formed on substrate when the sputterd atom hit the substrate and condenses. The plasma is maintained by emission of secondary electrons through the bombardment of the target and ionizes Ar atoms further. Permanent magnets are used in the system to increase plasma density by forming toroidal field. The advantage of RF sputtering is manily for insulating targets by providing no charge build up and less drive voltage to maintain the plasma. Structural properties are governed by the deposition

conditions during sputtering and can be controlled by maintaining the deposition parameters. These have strong influence on electrical properties of thin films. The deposition parameters that influence the film properties are the substrate temperature, argon sputtered pressure, RF power, and distance between the substrate and the target. The deposition conditions have been optimized to achieve the better crystallinity and surface properties.

BST thin films were grown first time in IIT Jodhpur by RF Magnatron sputtering technique. The objective of these experiments was to establish the process conditions which provide the best replication of the BST target stoichiometry. After reaching base pressure of $7x10^{-7}$ Torr by pumping the vacuum chamber with the Turbo molecular vacuum pump, sputtering gas (Ar) was admitted to the chamber via mass flow controllers, raising the chamber pressure to few mTorr. The target was pre-sputtered without any sample in the chamber for half an hour to remove any surface contamination. After achieving pre-conditioning of the sputtering target, BST films were sputtered on Si substrates with 2'' diameter target of $Ba_{0.5}Sr_{0.5}TiO_3$. To ensure good thermal contact with the substrate heater, the substrates were fixed to the heater block using silver paste. Before loading the substrate into the sputterer, the substrates were rinsed in acetone and de-ionised water and then baked at 100 ^{0}C for 10 minutes to remove any residual moisture. The substrate temperature was measured by a thermocouple inserted into the heater block. Ar flow was controlled in the range of 25-45 sccm. $Ba_{0.5}Sr_{0.5}TiO_3$ thin films were deposited on Si substrate at 600 ^{0}C and target to substrate distance was kept 4.5 cm. The thickness of the deposited films was achieved 250 nm thick. The deposition of $Ba_{0.5}Sr_{0.5}TiO_3$ layers was carried out in an argon atmosphere and the deposition pressure was kept around 15×10^{-3} Torr and the rf power was maintained between 70-75 W. The effect of deposition conditions on the structural properties has been discussed below.

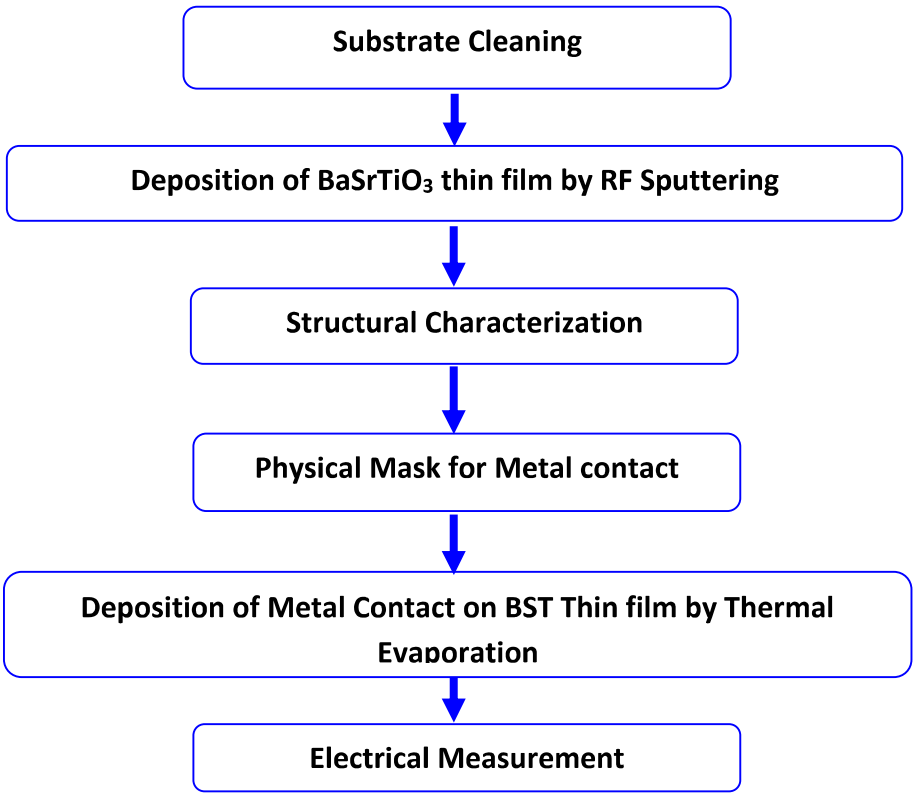

Figure 4.1: Schematic view of process flow for deposition of BST capacitor

4.2.1 Structural Analysis of BST Films

The structural order of a film is affected by the mobility of adsorbed surface atoms. Sputtering process has large impact on film comoposition since the process is governed by mass transfer and temperature. The atoms condense near the point of impingement and amorphous-like structure may be formed if the mobility is negligible. Since oxides have noticeably lower mobility of the atoms than metals at any temperature, hence lower temperature demonstrates less crystallisation. The sputtered BST thin films were characterized by XRD analysis to study the effects of Ar flow rate on the structural orientation of the thin films. However, the BST films deposited at 600°C are crystalline with well defined x-ray reflections as needed for obtaining better dielectric properties. The improvement at higher deposition temperature could be attributed to the fact that the thermal energy which the condensing species attain at elevated temperatures allowed for increased surface mobility and better nucleation and growth of the film. The BST films were deposited at different Ar flow rate of 25 sccm(standard cubic centimeter per minute), 35 sccm and 45 sccm and at constant deposition pressure of about 15 mTorr. The XRD patterns corresponding to the BST thin films as a function of Ar flows are shown in the Figure 4.2. The films show strong peaks at 31.80° along the (110) plane at all flow rate and indicated formation of BST phase of the thin films. It is observed that that the variation in Ar flow shows impact on structures of the BST thin films. Ar flow was increased from 25 sccm to 35 sccm and the peak intensity increased to a maximum and subsequently decreased at 45 sccm. The results show the good crystallinity and large grain size at the Ar flow of 35 sccm, observed smaller full width at half maximum (FWHM). By increasing the argon gas flow rate from 25 sccm to 35 sccm, BST (110) peak intensity is increased, while BST (100) and BST (200) peaks also appeared.

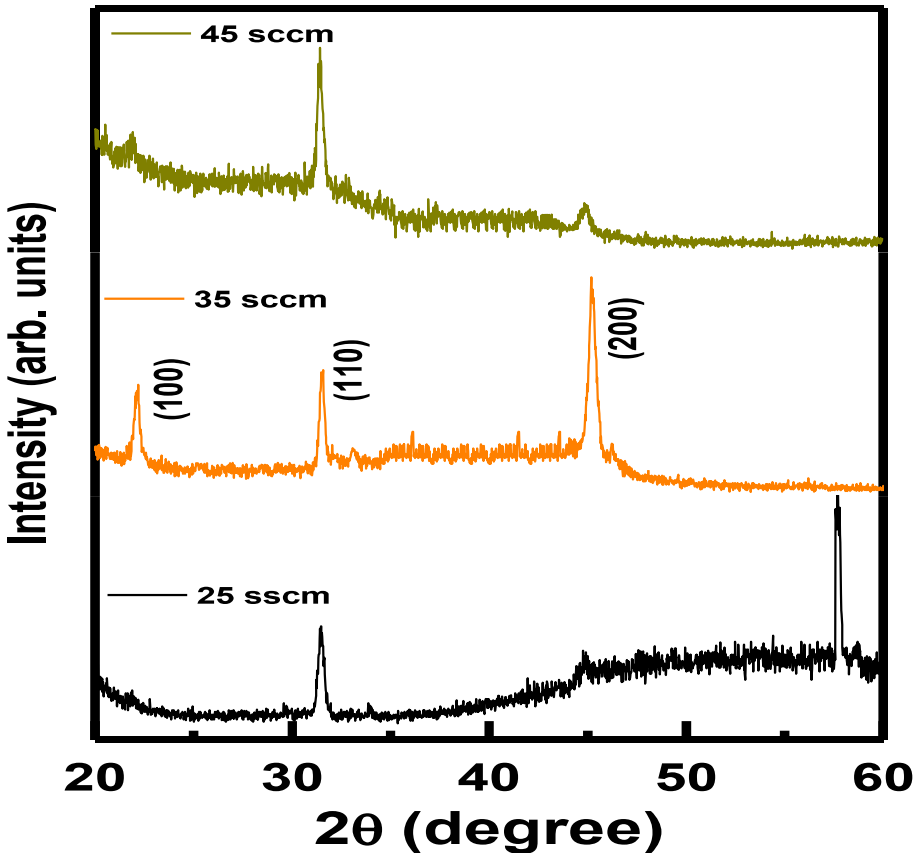

Figure 4.2: X-ray Diffraction patterns showing the effect of Ar flow rate on the crystallinity of BST thin films

Figure 4.3 shows the x-ray diffraction patterns of the films, which were deposited at various flow rate and post annealed at 800°C for one hour under ambient environment. All the films exhibited BST (100), (110) and (200) planes, shown in Figure 4.3. The films grown in the

low Ar flow rate were less crystalline and post deposition annealing was performed to improve the crystallinity. The x-ray diffraction pattern revealed that the structure of the annealed films was improved than un-annealed and no extra phase formation was reflected in the pattern. It is to be mentioned that increasing Ar flow rate could reduce the kinetic energy of sputtered particles. These particles at higher Ar flow rate have lower energy that results in much more defects such as oxygen vacancies in the BST thin film. The vacancies and structural changes are responsible to decrease the intensity of respective diffraction peak.

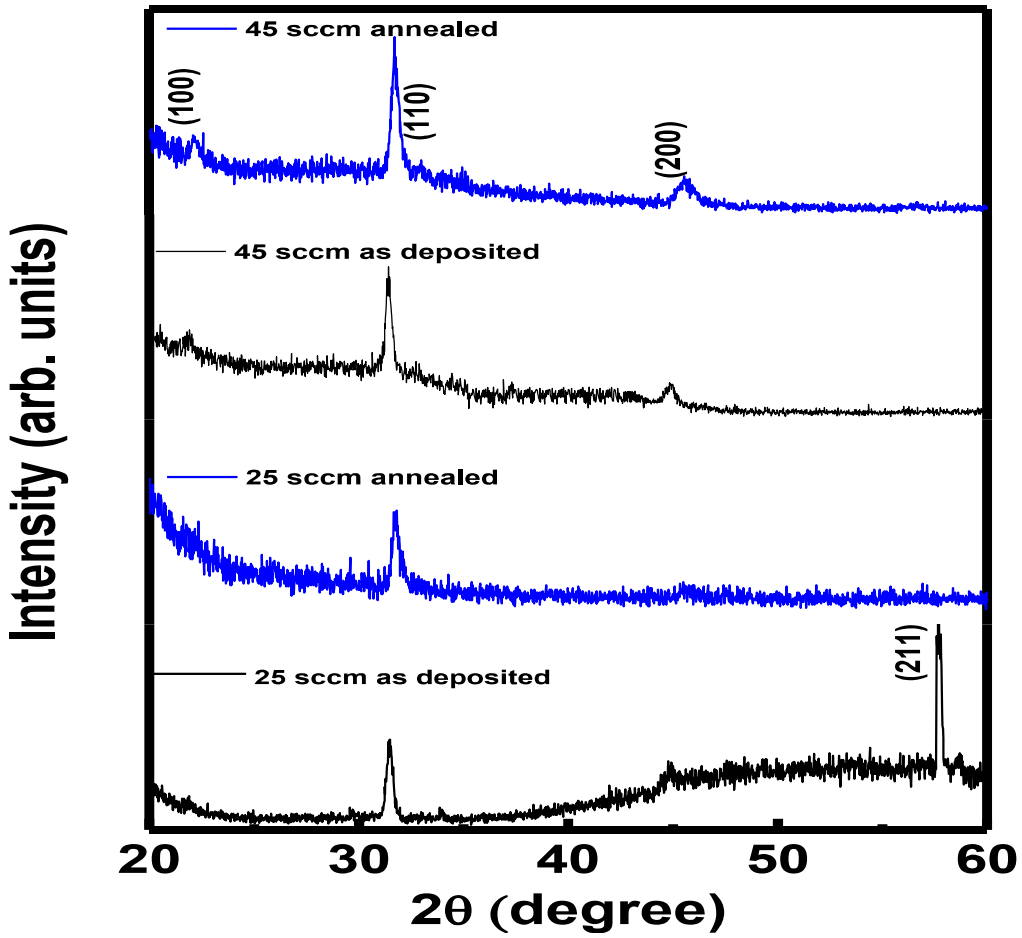

Figure 4.3: XRD spectra for as deposited and annealed BST samples at 25 sccm and 45 sccm Ar flow

4.2.2 Surface Morphology of BST Films

Surface characterization of the sputtered deposited BST thin films at different Ar flow conditions were carried out by Atomic Force Microscopy (AFM) technique. All the films were deposited at a substrate temperature of 600^{o}C. Many electronic properties are governed by surface roughness because of the carrier mobility and scattering which are dominated by level of surface roughness. In Figure 4.4, variation in surface roughness of the BST thin films under different Ar flow were observed. Figure 4.4 shows the root mean square (RMS) roughness of the BST thin films with sputtering power of 70 W, at various Ar flows of 25, 35 and 45 sccm. The BST films deposited at 25 sccm and 45 sccm have a surface roughness of 4.5 and 8.6 nm while the BST films deposited at 35 sccm has a surface roughness of 3.1 nm. The cation mobility on the growth surface reduces with higher flow rate, increases the grain size which in turn increases the surface roughness [Khojier *et al,* 2014]. This is because the energy of particles decreased with increasing the argon pressure, arriving at the surface, leaving less energy at the surface of the thin films due to collisions with more atoms [Yu *et al,* 2005].

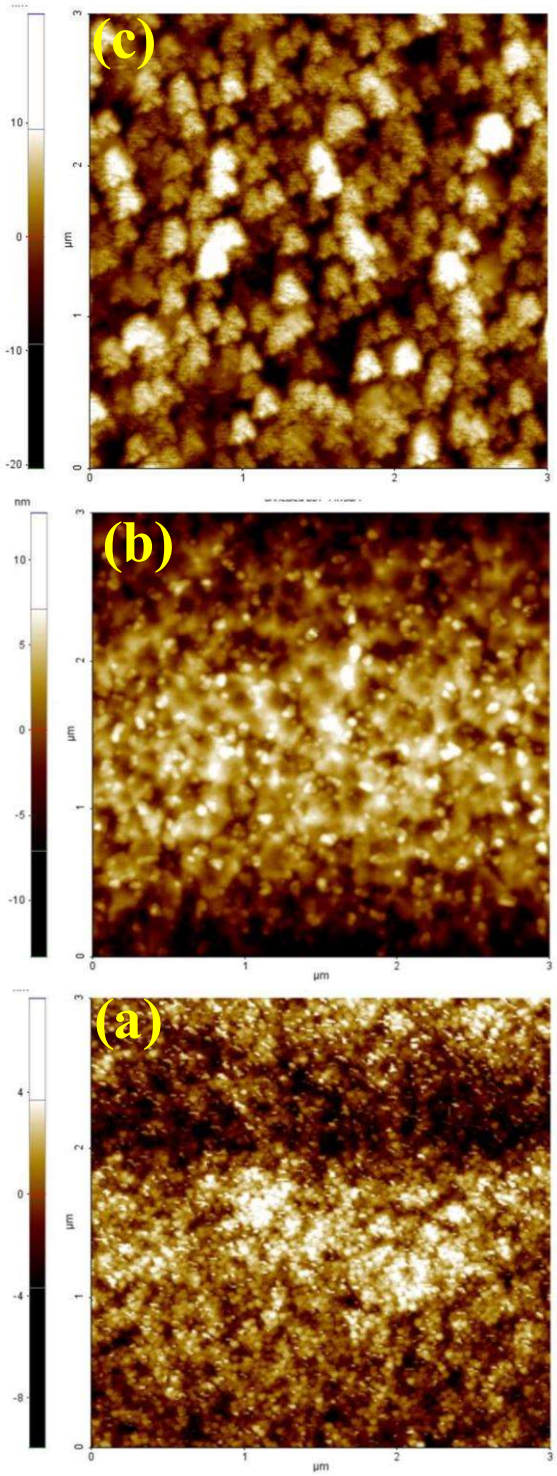

Figure 4.4: Surface morphology of BST Films Sputtered at different Ar flow rate (a) 35 sccm; (b) 25 sccm and (c) 45 sccm

4.2.3 X-Ray Photoelectron Spectroscopy Measurement

X-ray photoelectron spectroscopy provides information about the chemical bonding and valence states in a thin surface layer (≈10 ^{o}A) of a target material [Ohring, 1992]. In these experiments, a beam of incident x-ray photons ejects a core electron from an atom in the sample material; photoelectrons are ejected at a takeoff angle from the surface plane of the sample. The kinetic energy of the electrons is equal to the difference between the incident photon energy and the electron binding energy in the target. The measurements described in this section were performed at Material Research Center, MNIT Jaipur. Al Kα x-ray source (hυ = 1486.6 eV) was used as an excitation source with a base pressure below 1 x 10^{-9} mbar. For each of the series of films sputtered, a complete spectrum of data for ejected photoelectrons with energies in the

range 0 to 1400 eV was gathered. Compensation for sample charging was performed by comparison of the C 1s peak in each of the wide spectra with the known value (284.6 eV) of the adventitious C 1s peak. Shirley background was subtracted and a Voigt line-shape was used for the peaks to analyse the core-level spectra. Core level spectra with a 0.02 eV step size were gathered for the constituent elements in BST; a Ba *3d* spectrum from 775 to 800 eV, a Sr *3d* spectrum from 130 to 139 eV, and a Ti *2p* spectrum from 454 to 468 eV. Binding energies (BE) of Ba, Sr and Ti core levels of BST thin films were determined from the peak maxima of the spectra recorded by XPS.

Figure 4.5 shows the core level XPS spectrum of Ba atom in as grown BST film. The spin-orbit doublets of the Ba *3d* orbital is clearly seen for the film and the binding energies are about 778.1 eV and 793.7 eV corresponding to the Ba $3d_{5/2}$ and Ba $3d_{3/2}$ respectively. The observed binding energies coincides well with the earlier studies made on BST crystals and related to the Ba^{2+} state.

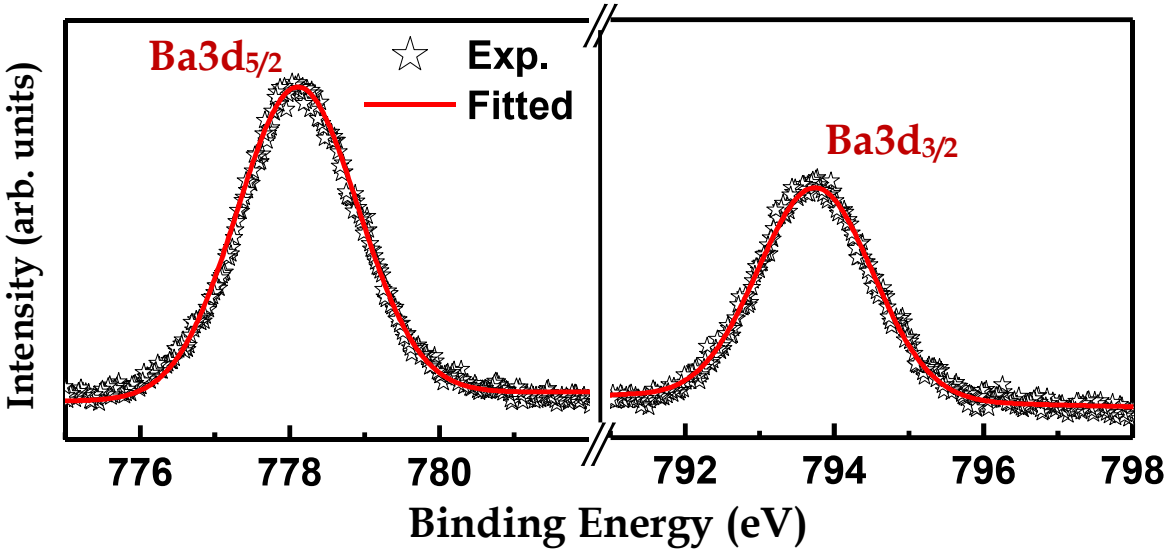

Figure 4.5: Core level spectrum of Ba 3d of BST thin film

The Sr3*d* spectra were fitted, which adequately represented by two overlapping Sr3*d* doublets (two Sr 3*d* SOS pairs), while a doublet splitting was observed 1.72 eV as similar to average of doublet splitting from the NIST XPS database. The binding energy peaks 132.69 eV (Sr $3d_{5/2}$) and 134.41 eV (Sr $3d_{3/2}$) as shown in Figure 4.6 are represented as perovskite BST phase from the pristine sample.

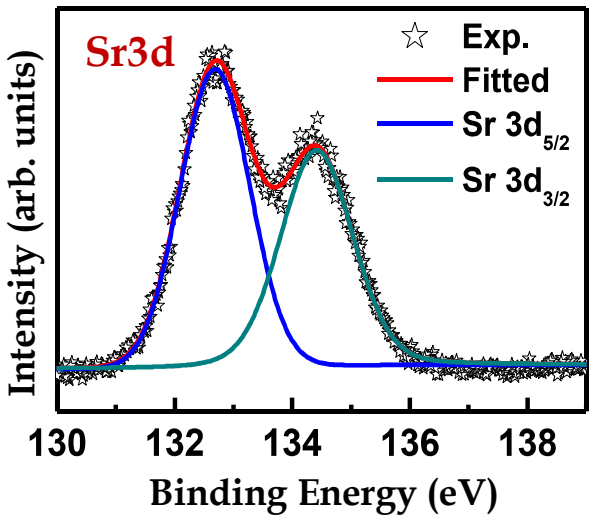

Figure 4.6: Core level spectrum of Sr 3d of BST thin film

Figure 4.7 shows the core level spectrum of Ti related to the 2p orbital. From the spectrum, spin orbit doublets of Ti2*p* at 457.54 eV and 463.20 eV are observed for $2p_{3/2}$ and $2p_{1/2}$ states respectively. Hence, the Ti *2p* spectrum confirms the oxidation state of Ti corresponds to the Ti^{4+} in the perovskite phase.

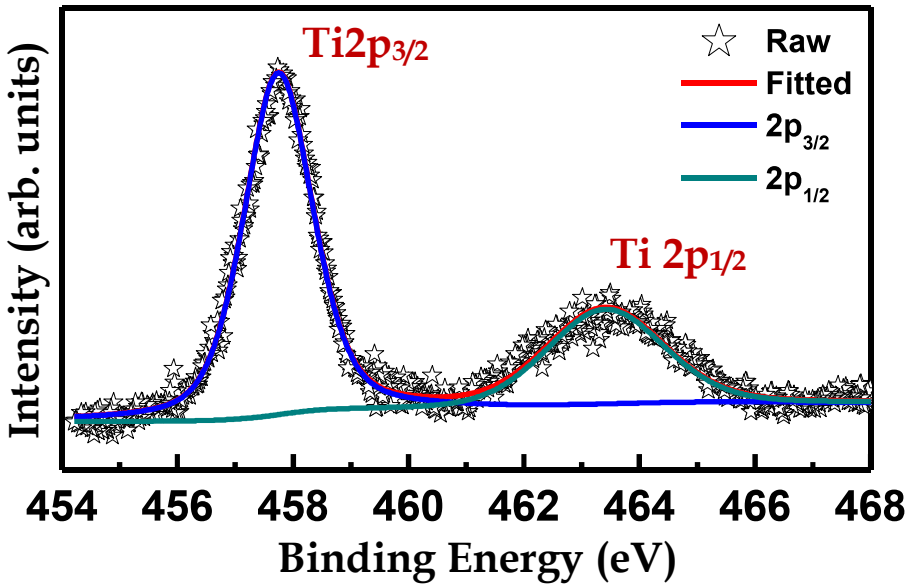

Figure 4.7: Core level spectrum of Ti 2p of BST thin film

4.2.4 Optical Characterisation of Pristine BST film

The optical band-gap energy is considered as one of the essential parameters for electro-optic materials. BST film was deposited by RF sputtering technique on quartz substrate for optical study. The transmittance was measured by UV-Vis-NIR spectrophotometer in the wavelength range of 200–850 nm. Figure 4.8 shows the standard measured transmission in the wavelength range of 200 to 850 nm for pristine $Ba_{0.5}Sr_{0.5}TiO_3$ thin film.

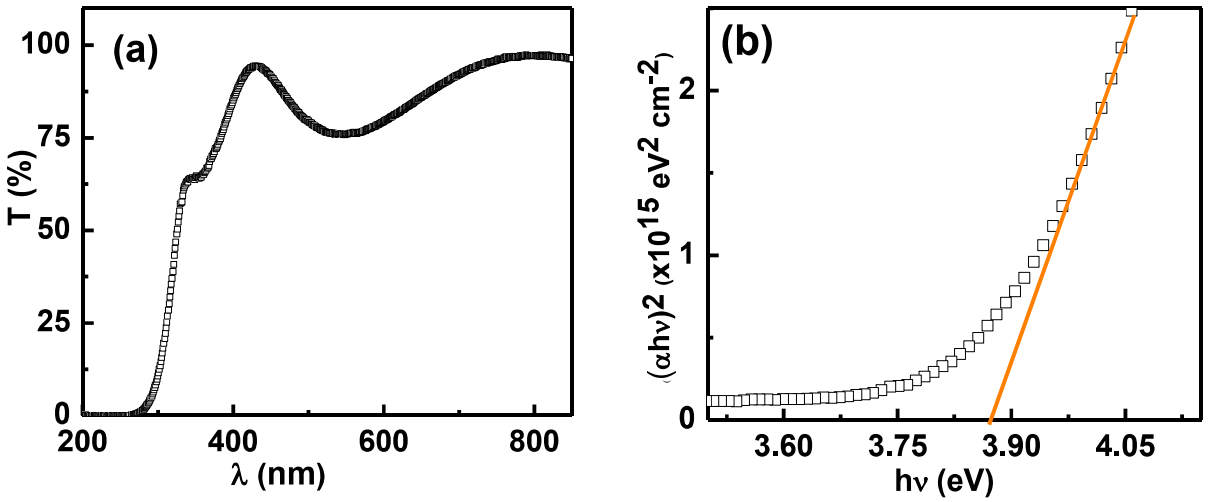

Figure 4.8: Optical spectra (a) Measured Transmittance (b) Estimated band gap of Pristine BST film

The optical band-gap 'E_g' has been determined from the measured transmittance curves using the Tauc relation.

$$(\alpha h\nu) = C\,(h\nu - E)^r \qquad (4.2)$$

where α is the absorption coefficient, C is a constant, incident photon energy hν and r =0.5, 1.5, or 2 for allowed direct, forbidden direct, and allowed indirect electronic transitions, respectively. The band gap energy (E_g) has been determined with consideration of an allowed direct transition i.e. r = 0.5 between the valance band and conduction band. Figure 4.8 shows an optical transmittance plot between hυ vs $(\alpha h\upsilon)^2$ and band gap E_g was determined from an intercept on the energy axis hυ. The band-gap of the BST films with was determined approximately 3.87 eV, which is similar to reported by Xu et al [Xu *et al*, 2005].

4.2.5 Dielectric Properties

BST material is characterised with non linear response, shows a typical dependence of dielectric constant on electric field. It is to be mentioned that dielectric measurement is often carried out by using ac signal and the dc field bias across the sample under test. Ni top electrodes were deposited by using thermal evaoporation to make capacitor devices. A vacuum pressure below 10^{-7} Torr was kept to ensure a large mean free path and prevent oxidising of the atoms. A tungesten wire source was used to evaporate Ni granulates. Top electrodes were produced of 200 nm thickness of Ni through a physical mask of 400μm in diameter. The schematic view of the BST varactor is shown in Figure 4.9.

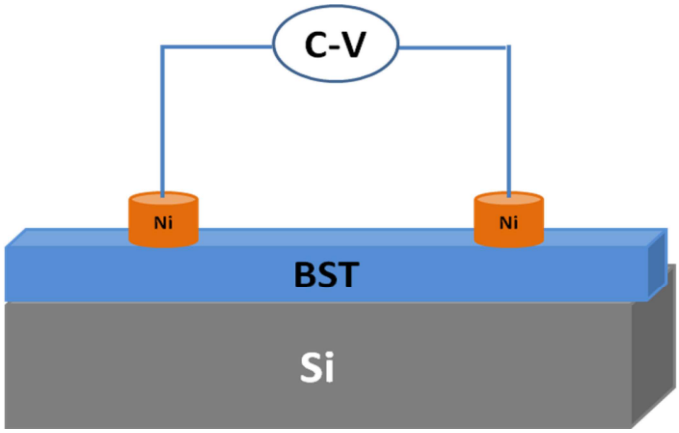

Figure 4.9: Schematic illustration of the fabrication of Ni/BST/Si varactor

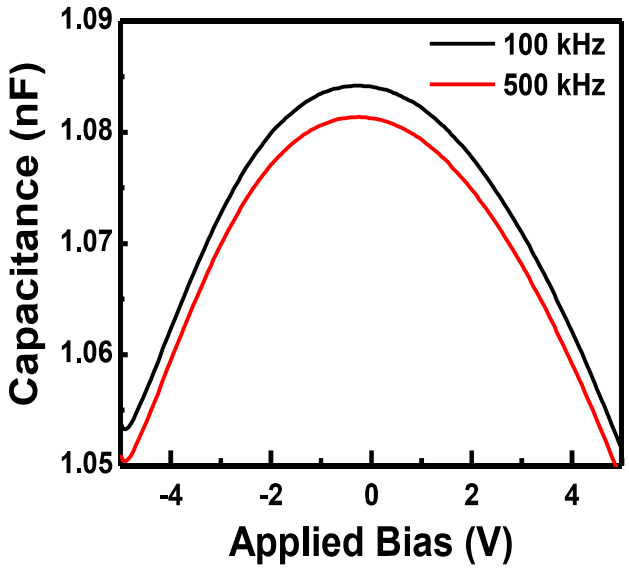

Figure 4.10: Capacitance voltage characteristic of BST varactor

The features of tunable ferroelectric material are useful for frequency-agile microwave devices. Depending upon the requirements, capacitors are being formed by using dielectric layers of ferroelectric materials. The capacitance of dielectric materials corresponds to dielectric constant. Therefore, the capacitance on BST based capacitor has been measured using Kiethley SCS 4200 to perform C-V measurement. It is shown in Figure 4.10 that the capacitance of BST capacitor is changes by applied voltage as expected bell shaped behavior of BST perovskite film.

Metal contact on Si-based technology, forms an ohmic contact as it is required for every semiconductor device in order to drive current in and out of the device. On the contrary, it is desirable to have the largest barrier possible to avoid residual leakage currents for the usual applications of ferroelectric capacitors. Leakage current is one of the limiting factors for the suitability of a dielectric material for frequqncy filter and tunable device applications [Saha and Krupanidhi, 2000]. Conduction mechanism of BST thin films is primarily through Schottky emission in which leakage currents are controlled by the barrier height [Hwang *et al*, 1998]. The leakage current characteristics were measured using configuration of Ni/BST structure as shown in Figure 4.11, similar to reported by Joo et al. [Joo *et al*, 1997]. The observed small current in the order of few nA for BST capacitor, considered good for tunable device application.

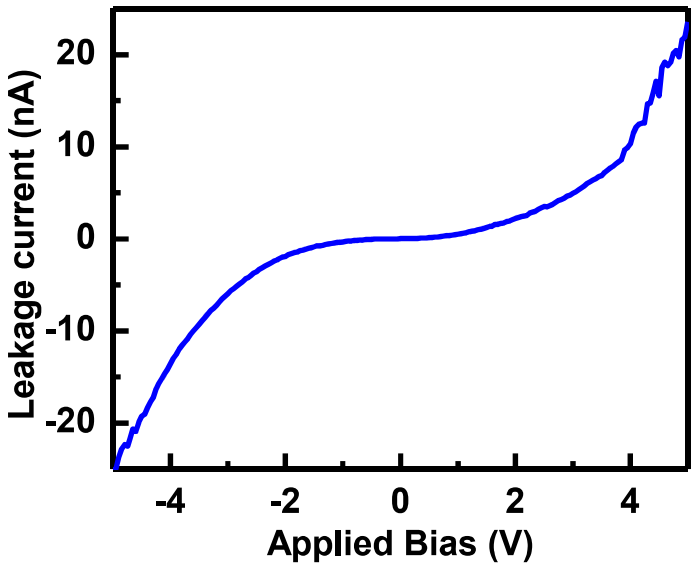

Figure 4.11: Leakage current of pristine BST varactor

4.3 GAMMA RADIATION INDUCED EFFECTS ON BST FILMS

The physical properties of the materials are altered by high-energy gamma irradiation. In contrast to the interaction of charged particle, the interaction of gamma radiation is primarily through photoelectric effect, Compton scattering and formation of electron-positron pair. It is expected that ionising radiation causes structural defects on the exposure to gamma-rays [Zhu, 1998]. The changes are strongly dependent on the structure of the exposed material.The lowest threshold energy is about 58 keV for displacement of in-plane atoms is known to correspond to the displacement of in-plane oxygen [Tolpygo *et al*, 1996]. The energy transferred to a material by ionizing radiations is quantitatively characterized by the absorbed radiation dose and the SI unit of dose is Gy. The influence of radiation depends on the dose and the level of degradation is higher for the higher dose [Tanassova *et al*, 2001].

4.3.1 Structural Analysis of Gamma Irradiated BST Films

In order to study the effect of gamma radiation, we have investigated the structural properties of BST thin films deposited on Si substrate at different gamma doses. The films were irradiated in gamma chamber varying the gamma doses from 0 kGy (pristine) to 200 kGy to

study the effect phase and structure of the films. Figure 4.12 shows x-ray pattern in 2θ-ω scans of BST film deposited at 600 ^{0}C. It was observed that the pristine film has perovskite structure and various BST peaks are seen clearly from the spectra. It is noted from the figure that there is change in full-width-at half-maximum (FWHM) and intensity of BST films irradiated with gamma radiation, advocating a relaxation in film surface due to defect in the film with respect to un-irradiated films.

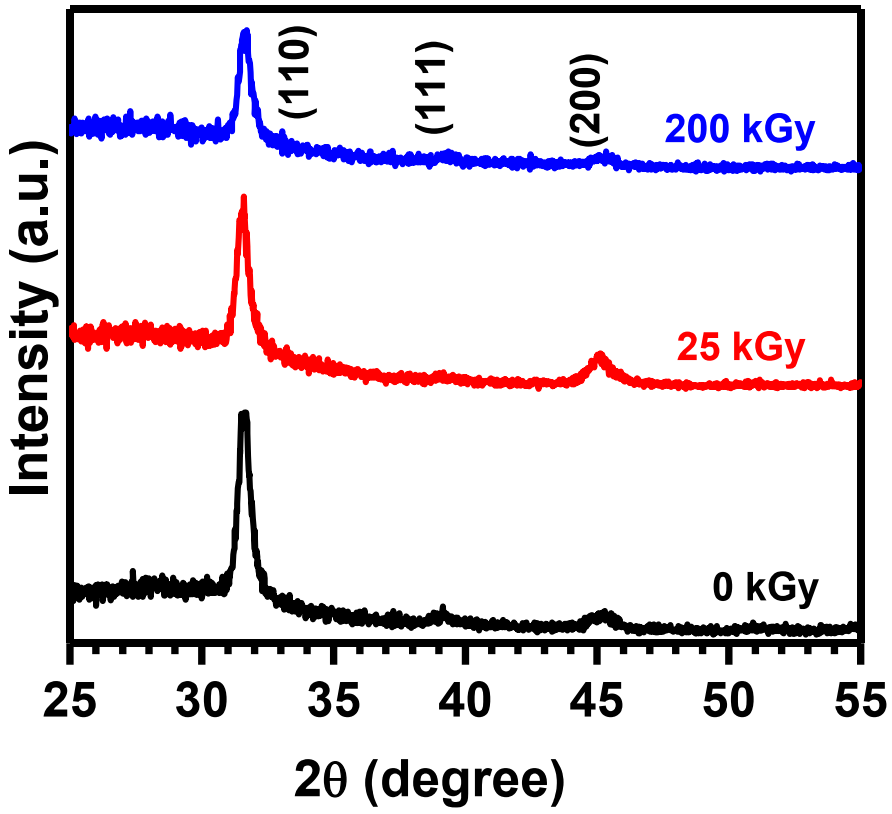

Figure 4.12: Gamma irradiation effects of BST structure

A common defect in perovskite oxide films is oxygen vacancy site which has a net positive value and causing distrortion by repelling the Ba, Sr, and Ti atoms in the structure. Moreover, the FWHM of the (110) peak increases from 0.42^0 to 0.50^0 with increases gamma dose in turn reduces the crystallinity slightly of the BST film after gamma irradiation. It is likely that irradiation allows generation of oxygen vacancies resulting in the increase of FWHM. The result suggests that gamma irradiation has a remarkable effect on the film structure which leads to an increase in oxygen vacancies, hence yielding surface relaxation in the gamma irradiated film. The presence of defects after gamma irradiation also decreases the intensity of the diffraction peaks which confirms the reduced crystallinity of the film.

4.3.2 Surface Morphological Study

The AFM images recorded for the gamma irradiated BST thin films, exposed to different gamma doses, shown in Figure 4.13. These images show that the as-deposited thin film observed smooth as compared to gamma irradiated films. The gamma exposed films become more rougher with the increase of the gamma radiation dose showing partial contribution of radiation induced defects along with the formation of large sized clusters with voids. The surface roughness was observed from 2.4 nm of the pristine to 4.4 nm for 200 kGy BST sample. The gamma radiation induces defects are produced during its passage through the film which reults into slight disorder in the film structure.

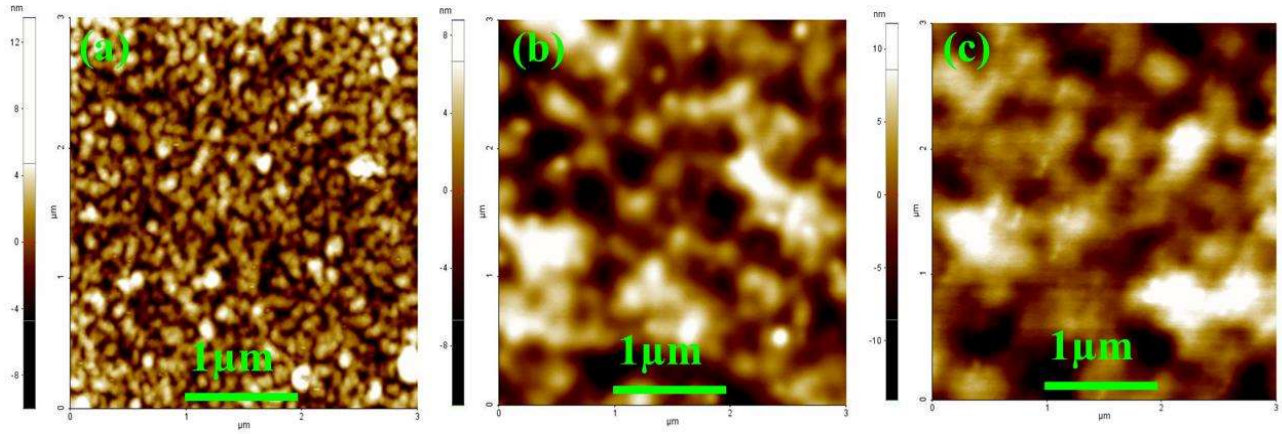

Figure 4.13: AFM spectra of BST films (a) Pristine, (b) 25 kGy, (c) 200 kGy.

4.3.3 Core Level and Valence Band Photoelectron Spectroscopy

The surface microscopic structures and electronic properties are important for better device performance and gives insights into fundamental mechanisms of material interface. The energy level alignment at interfaces can be affected by the surface chemistry of the film. The surface chemical states of an atom can be examined by using core level and valence band spectra. The core level themselves are measurably shifted by changes in the distribution of valence electrons and chemical shifts are measured by x-ray Photoelectron Spectroscopy (XPS). Core level energy, energy shift and related properties are of importance for the rapidly developing field of surface and interface engineering. Surface treatment for $BaTiO_3$ and $SrTiO_3$ thin films showed that the position of the oxide core levels and valence-band maximum is changed by the treatment [Amy *et al*, 2004]. Considerable progress has been carried out to understand the physics of core-level photoemission from surface atoms of BST however effect of gamma irradiation on the surface electronic properties and even the core level spectra of such complex oxide is still uncertain. High energy radiation induced structural changes in device material are found to be associated with the change in the atomic concentration due to bond breaking and its possible reorganization after irradiation [Rai *et al*, 2010]. Therefore, it is expected that gamma treatment may affect the electronic structures of core-level and valence band maxima of BST films. In addition electrical and optical properties are also correlated to the surface properties. In the present study, we have investigated the surface chemical states of gamma-ray irradiated BST thin films by XPS. XPS spectra were acquired on pristine, 25 kGy and 200 kGy samples. XPS analysis was carried out to identify the chemical bonding energies of constituting elements of the BST thin films.

Further, gamma-ray treated BST shows asymmetry towards higher energy which indicates radiation induced changes [Rai *et al*, 2010], in near surface region of BST thin films, similar to HfO_2, reported by Cheng *et al* [Cheng *et* al, 2013]. Figure 4.14 shows the Ba*3d* photoemission core level spectra of gamma-irradiated BST at gamma doses of 0 kGy, 25 kGy and 200 kGy. The binding energy peaks at 778.1 eV (Ba $3d_{5/2}$) and 793.7 eV (Ba $3d_{3/2}$) are assigned to Ba in perovskite phase. Higher binding energy shifts of about 1.15 eV was observed for Ba atoms with increasing the dose (200 kGy) of gamma-ray irradiation.

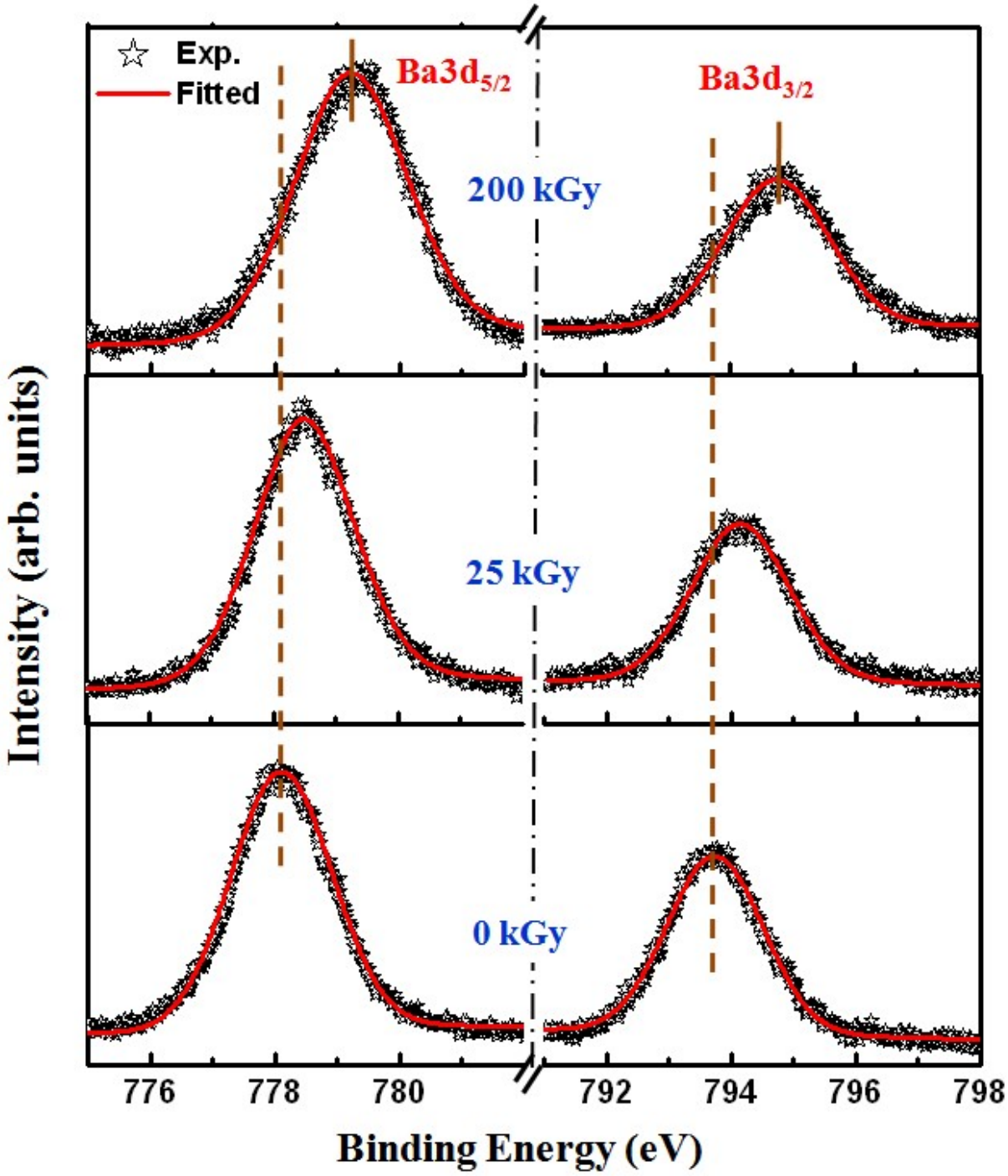

Figure 4.14: XPS core level spectra of Ba3*d* ($3d_{5/2}$ and $3d_{3/2}$) of gamma irradiated BST thin film from 0 kGy (Pristine) to 200 kGy.

Figure 4.15 shows the Sr3*d* photoemission core level spectra of gamma-irradiated dose of 0 kGy, 25 kGy and 200 kGy. The Sr3*d* spectra were fitted, which adequately represented by two overlapping Sr3*d* doublets (two Sr 3*d* SOS pairs), while a doublet splitting was observed 1.72 eV as similar to average of doublet splitting from the NIST XPS database. The binding energy peaks 132.69 eV (Sr $3d_{5/2}$) and 134.41 eV (Sr $3d_{3/2}$) are represented as perovskite BST phase from the pristine sample as shown in Figure 4.15. The core level spectra are shifted of about 1.12 eV towards higher binding energy for Sr 3d atoms at 200 kGy gamma-ray irradiation dose with respect to pristine.

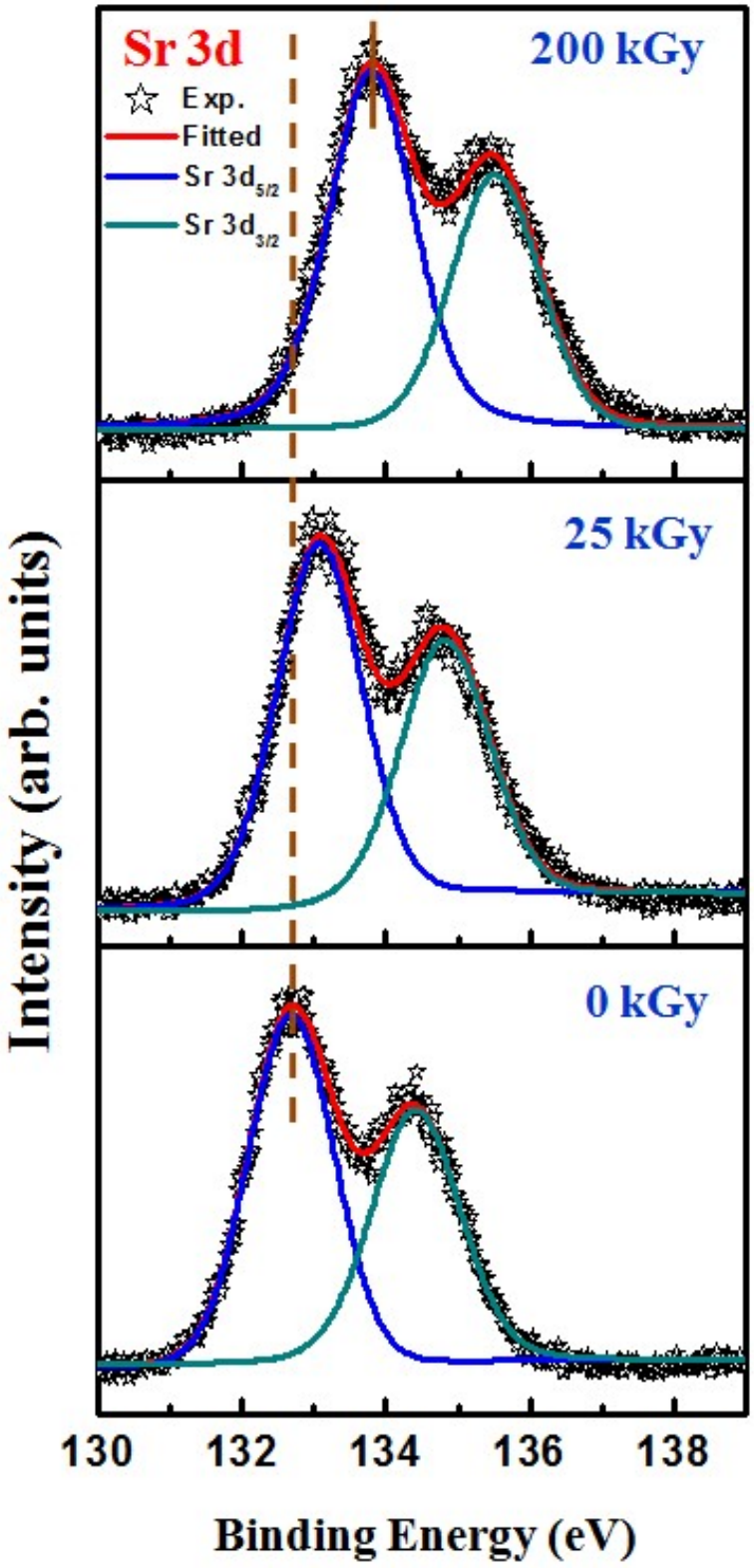

Figure 4.15: XPS core level spectra of Sr3*d* ($3d_{5/2}$ and $3d_{3/2}$) of gamma irradiated BST thin film from 0 kGy(Pristine) to 200 kGy.

Figure 4.16 shows XPS core level spectra for different states of Ti atom such as Ti$2p_{3/2}$ and Ti$2p_{1/2}$ for the pristine and gamma ray irradiated BST. Ti$2p$(Ti^{4+}) peaks are observed at 457.54 eV and 463.20 eV corresponding to $2p_{3/2}$ and $2p_{1/2}$ for pristine BST sample. No shoulder was observed at lower binding energy side of Ti2*p* spectra, attributes Ti^{+3} species i.e. Ti^{3+} $2p_{3/2}$ (455.0 eV) and Ti^{3+} $2p_{1/2}$ (461.7 eV) [Moulder *et al*, 1992], neither before nor after gamma exposure. Further, gamma-ray treated BST shows asymmetry towards higher energy which indicates presence of radiation induced changes and core level peak is shifted 1.17 eV towards higher binding energy at 200 kGy gamma dose.

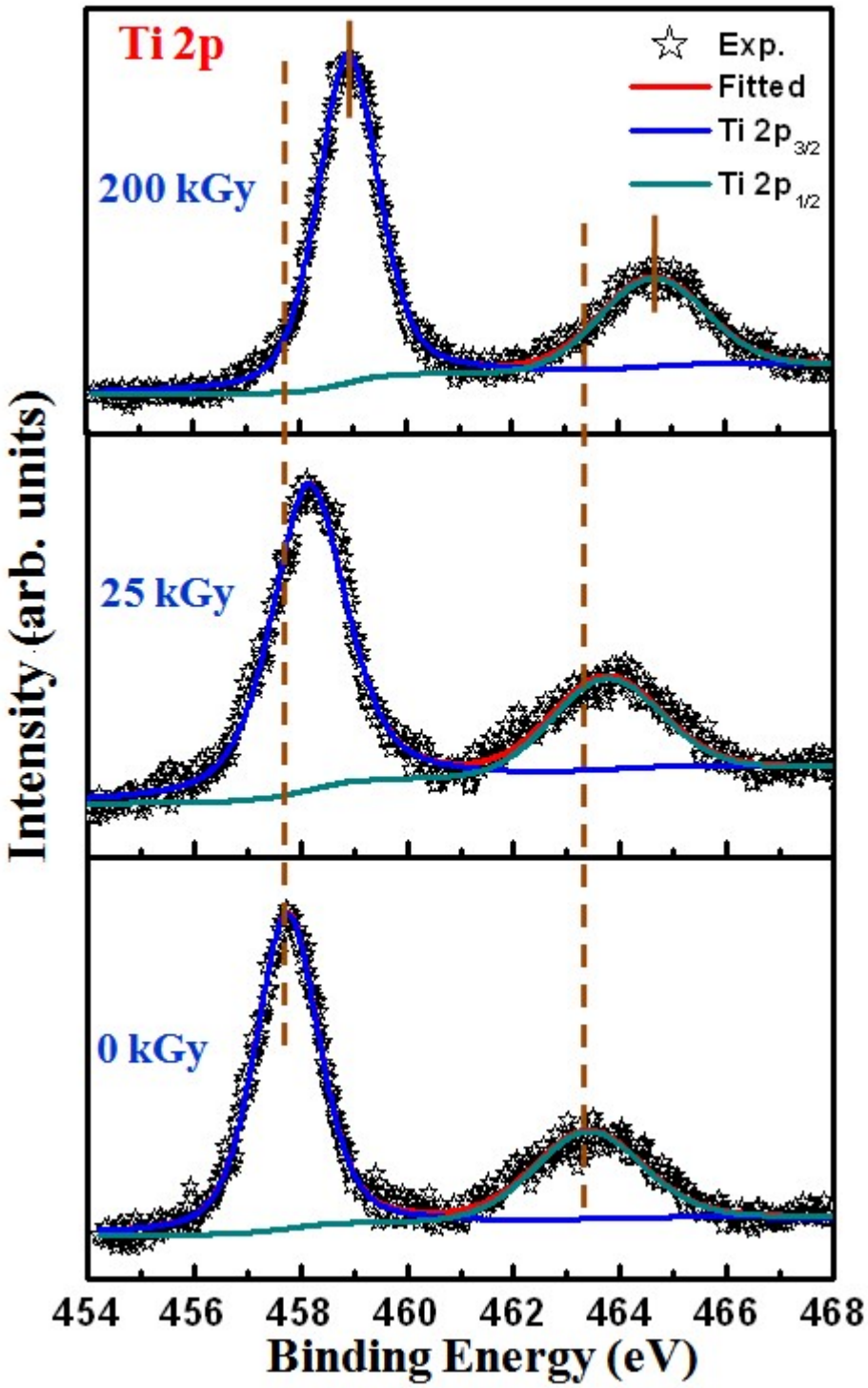

Figure 4.16: XPS core level spectra of Ti $2p_{1/2}$ and $2p_{3/2}$ of gamma irradiated BST thin film from 0 kGy(Pristine) to 200 kGy.

Therefore it has been observed that higher binding energy shifts of about 1.1 eV was found for the all Sr, Ti and Ba atoms with increasing the dose of gamma-ray irradiation. The higher binding energy shift in core level of Ba, Sr and Ti elements in gamma irradiated BST can be attributed to the variation in chemical environment of the elements or relaxation effect [Cracium and Singh, 2000; Mukhopadhyay and Chen, 1995; Li *et al,* 2005]. There could be an involvement of the Fermi level (E_F) shift [Wang *et al,* 2006] apart from chemical and relaxation, since the original Fermi level of BST could be shifted because of radiation induced changes in the film after gamma irradiation. The shift in the Fermi level of gamma exposed BST film would contribute to the shift in BE, while undergoing an equilibration process with BST through space

charge effect [Halder *et al*, 1999]. Therefore, it is important to investigate the effect of gamma irradiation on the Fermi level E_F, in addition to the analysis of core level spectra. This has been studied through valence band edge spectra of the pristine and gamma treated BST as shown in Figure 4.17. The energy of the valence band maxima is determined from the intercept of a linear fit with a zero line. The top of the valence band is positioned at about 2.0 eV lower than the Fermi level for pristine BST thin film as shown in Figure 4.17.

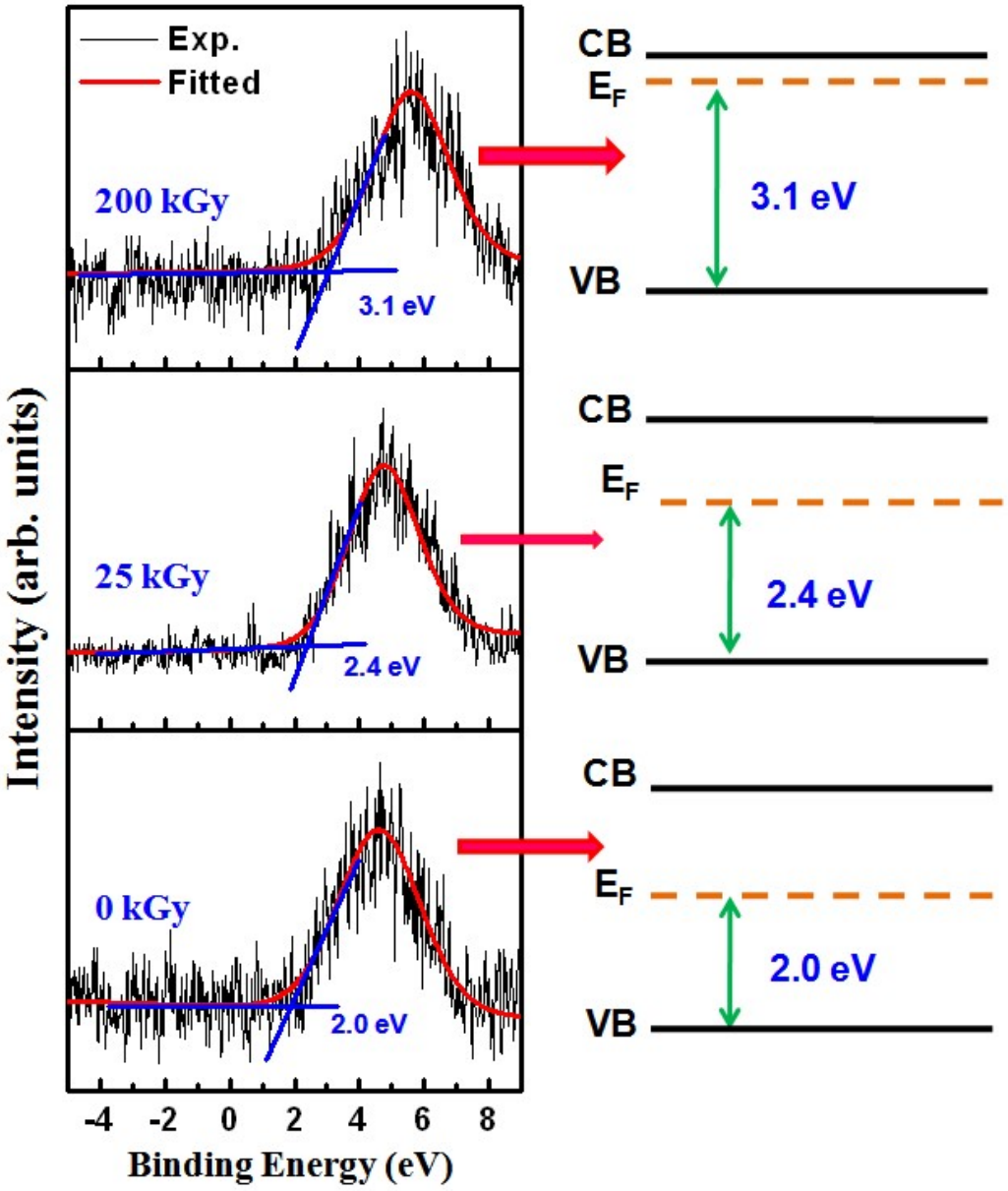

Figure 4.17: XPS valance band spectra of BST thin film from 0 kGy(Pristine) to 200 kGy and schematic reprentation of Fermi level shift.

It can be clearly seen that the position of the Fermi level is shifted towards conduction band by ~1.1 eV in the gamma irradiated BST at 200 kGy with respect to pristine. The shift in core level BE position is an appearance of Fermi level shift due to irradiation rather than the usual chemical shift occur to any change in the chemical environment. This result seems to be consistent with the energy shifts in Ba, Ti and Sr core levels, which is correlated to the higher Fermi level in the BST films. Gassenbauer *et al* demonstrated a shift of the valence and conduction band edges due to band bending with respect to the Fermi level which was defined by a shift of the complete spectra including all core levels and valence bands [Gassenbauer *et al*, 2006] of tin-doped In_2O_3. The gamma ray treatment raised the E_F level toward the conduction

band edge by 0.4 eV and 1.1 eV for 25 kGy and 200 kGy doses respectively from that of the pristine BST as demonstrated in Figure 4.17. An increment in E_F leads to a noticeable increase in binding energy for all core level peaks because E_F is considered a reference for the scale of binding energy in XPS. The concentration of free electrons increases with increasing density of irradiation-induced defects, act as donors in these materials. Therefore, in our BST samples donor-like defects are predominantly generated during irradiation, shifting E_F upward. Since the chemical shift could not be reflected from any of the core level spectra thus there is direct link between the gamma irradiation in BST and the E_F position where gamma irradiated BST materials will be more n-type in character.

4.3.4 Optical Properties of Irradiated BST Thin Film

Optical properties of thin films are affected by the defects, compositions and microstructural variations. Therefore, transmission measurement can be correlated to structural, microstructural and chemical composition. A change in optical band gap of BST film has been reported due to oxygen vacancy defects as well as changes in stoichiometry and strain. In the present study the BST thin film was irradiated with ^{60}Co gamma radiation doses from 0 kGy (pristine) to 200 kGy. The band-gap of the pristine $Ba_{0.5}Sr_{0.5}TiO_3$ films was observed approximately 3.87 eV.The estimated values of E_g did not show any significant change in the band gap as shown in Figure 4.18 however slight change towards decreasing E_g by 0.07 eV was observed upon irradiation. This favors to high optical tolerance of BST thin films against gamma irradiation.

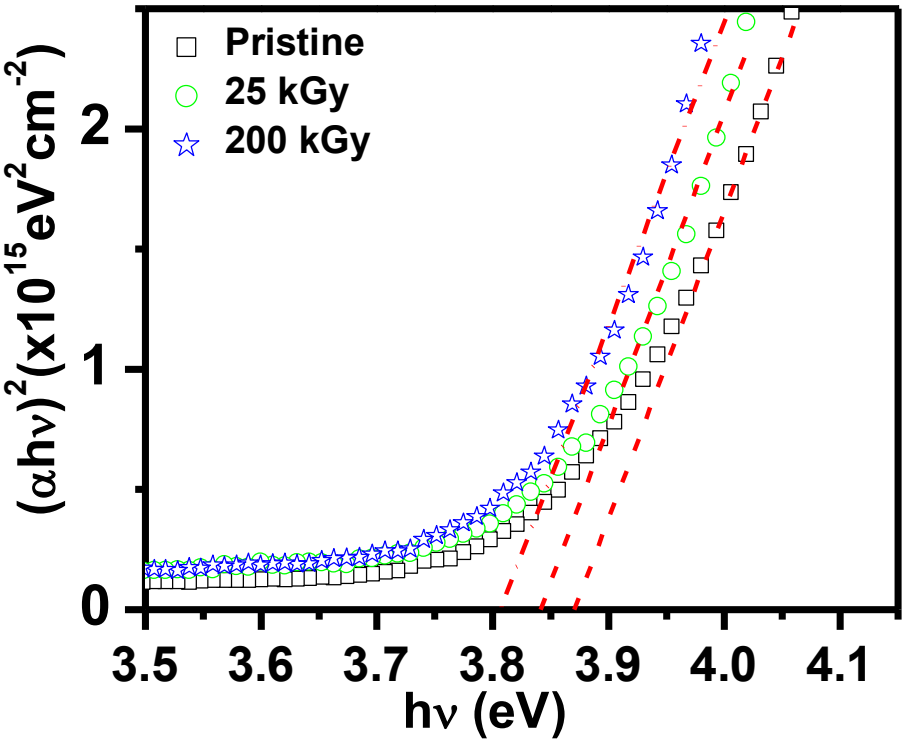

Figure 4.18: Optical band gap of the gamma irradiated BST film

4.3.5 Leakage Current Study

The leakage current characteristics of Ni/BST/Ni (MIM) capacitor were measured at room temperature and shown in Figure 4.19. It can be seen that leakage current increases with gamma-ray doses [Miao *et al,* 2009], which also favour gamma-ray induced changes in the surface core level state of Ti, Ba and Sr. Dih *et. al.* have reported the role of oxygen in increasing the conductivity because of the associated electrons with the oxygen vacancies [Dih *et al,* 1978]. The increase in the leakage current after gamma irradiation, reduction may be expected to be caused by the migration of oxygen from the surface as well as loss from the bulk. The similar behaviour was observed in glass by treatment with gamma ray irradiation [Rai *et al*, 2010],

accompanied with decrease in oxygen content after irradiation [Raja *et al*]. The gamma treated BST contains some missing oxygen ions, where electrons are generated to maintain the electrical neutrality [Rajopadhye *et al,* 1987] which makes films relatively n-type compared to pristine BST. The observed behaviour of a BST-based capacitor comprises the contributions from the polarization loss and electronic conduction [Tsai *et al*, 1997]. Upon increasing the gamma doses, the leakage current increases rapidly due to an increase in the electron concentration that result in increased conductivity. A simple charge transfer model can be applicable to understand an increase in the current density with the gamma radiation dose [Arshak and Korostynska, 2006]. Accordingly, the upward shift in Fermi level of the gamma exposed thin films with respect to as-deposited, results in lowering of the conduction barrier.

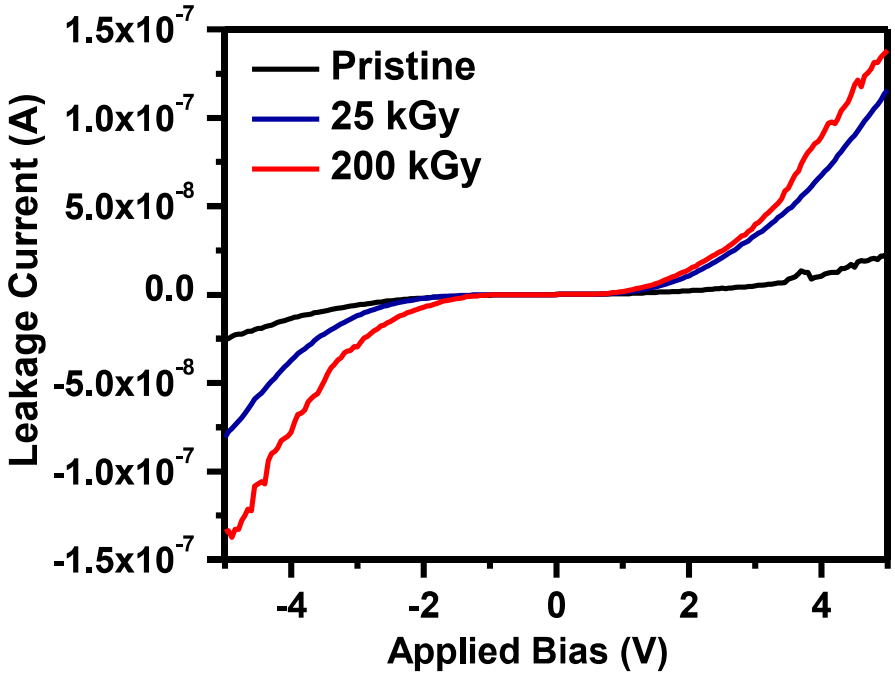

Figure 4.19: Leakage current of Ni/BST/Si device at 0, 25 and 200 kGy.

4.4. CONCLUSIONS

The chapter focuses on optimization of the $Ba_{0.5}Sr_{0.5}TiO_3$ film growth parameter using RF sputtering technique including Ar flow rate and deposition tempertaure. Further, BST thin films were investigated as a function of gamma irradiation doses. Gamma radiation induced structural and surface morphological changes were observed in comparison with pristine sample. The crystal structure showed increasing FWHM of diffraction peak with higher gamma dose and surface roughness was found to increase due to gamma radiation induced effects on BST films. X-ray photoelectron spectroscopy showed that gamma ray treated BST surface layer exhibits an increase in the surface core-level features by 1.1 eV towards higher binding energy of Ba, Sr and Ti atoms which are consistant to Fermi level shift. Dielectric properties were measured on Ni/BST/Si configuration and characteristic bell shaped C-V behavior was observed along with small leakage current. The radiation induced phenomenon gave variations of electronic rearrangement and responsible for the increase of leakage current in the gamma irradiated BST thin film.